11th International Symposium on Turbulence and Shear Flow Phenomena (TSFP11)
Southampton, UK, July 30 to August 2, 2019

THE COMPETITION BETWEEN TURBULENT AND MOLECULAR DIFFUSION IN PLASMA MIXING LAYERS UNDER COMPRESSION

Giovanni Viciconte
CEA, DAM, DIF, F-91297 Arpajon, France
giovanni.viciconte@cea.fr

Benoît-Joseph Gréa
CEA, DAM, DIF, F-91297 Arpajon, France
benoit-joseph.grea@cea.fr

Fabien S. Godeferd
LMFA UMR5509-CNRS Université de Lyon,École centrale de Lyon,UCBL, INSA Lyon
Écully, France
fabien.godeferd@ec-lyon.fr

ABSTRACT

In order to characterize the turbulent mixing produced at the fuel/ablator interface of compressed capsules relevant to inertial confinement fusion (ICF), we perform direct numerical simulations accounting for non-uniform transport coefficients typical of plasma mixtures. It is shown that during the implosion, mixing layers growths can be successively determined by turbulence and molecular diffusion depending on initial conditions. This phenomenon leads eventually to the relaminarization of the layer, provoking the sudden diffusion of heavy materials toward the center of the capsule.

INTRODUCTION

A fundamental problem in inertial confinement fusion (ICF) is to quantify the mixing produced from hydrodynamics instabilities at the fuel/ablator interfaces which eventually deteriorate the capsule yield (Betti & Hurricane (2016); Remington *et al.* (2018)). During the implosion, the materials enter a plasma state due to the extreme conditions reached in order to achieve fusion.

The tremendous temperature increase implies very strong temporal and spatial variations of viscosity and molecular diffusion (Braginskii (1995); Ticknor *et al.* (2016)), eventually having important consequences on the mixing. It has already been shown by Weber *et al.* (2014) that the viscosity growth leads to an enhanced dissipation of small scales of turbulence developing in the fuel. Davidovits & Fisch (2016) further ask if this mechanism, as occurring suddenly, can be exploited in order to transform turbulent kinetic energy into heat favoring fusion reaction. In addition, Zylstra *et al.* (2018) suggests that there may exist implosion configurations where the molecular diffusion appear to be the main ingredient explaining mixing.

However, the questions of how the variation of the transport coefficients influences mixing zone dynamics and whether it has to be accounted for in numerical simulations are still pending. In order to investigate these effects, we propose numerical simulations of variable density mixing, using the plasma viscosity and diffusivity model from Arnault (2013). We compare these results with constant transport coefficients simulations, highlighting differences in multiple quantities. Finally, we show how the diffusion of the mixing layer is affected by the competition between turbulent and molecular diffusion depending on the initial Reynolds number.

SIMULATION SETUP

Our analysis starts from the compressible Navier-Stokes equations(see Vold *et al.* (2015)) for momentum ρU_i, mass ρ, mass fraction of species α, Y_α, temperature T and n number density of particles in a Cartesian stationary reference frame . We consider a binary mixture between deuterium-tritium (DT) and ablator (CH) governed by:

$$\frac{1}{\rho} = \frac{Y_{DT}}{\rho_{DT}} + \frac{Y_{CH}}{\rho_{CH}}$$

where ρ_{DT} and ρ_{CH} are respectively the microscopic densities of the light and heavy materials. They are defined as

$$\rho_{DT} = \frac{nM_{DT}}{1+Z_{DT}} \quad \text{and} \quad \rho_{CH} = \frac{nM_{CH}}{1+Z_{CH}}$$

where Z_α and M_α are the material ionization number and atomic mass.

Following other works on isotropic compression (Rogallo (1981), Cambon *et al.* (1993), Davidovits & Fisch (2016)), we decompose the solution into a base flow and perturbation. The base velocity U_i^B is chosen as a compressible background flow on the form:

$$U_i^B(\mathbf{x},t) = -S(t)x_i \tag{1}$$

where the compression time rate $S(t)$ is spatially uniform. All the other base components can be characterised in a closed analytical form, provided that we use some hypotheses. In particular we study the case where the base density ρ^B is uniform in space and depend only on time. The

time evolution of base flow temperature, pressure and density at the center of the domain is plotted in figure 1, together with R, the normalized size of the domain (that we call compression parameter). These values are consistent with those typically encountered in ICF application. Within

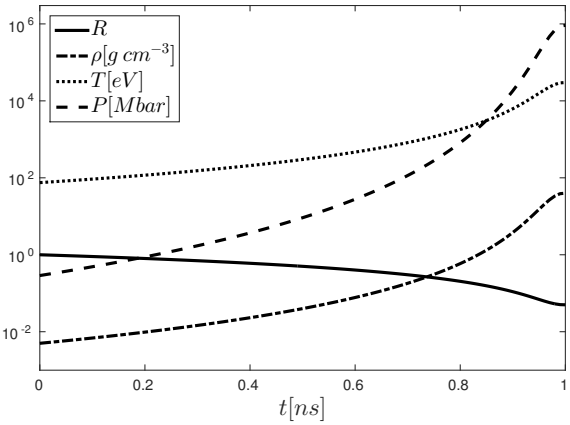

Figure 1: Evolution of density, temperature and pressure of the base flow at the center of the domain. In black the evolution of the compression parameter $R(t)$ is also plotted.

this framework we can derive the following equations for the perturbations.

$$\partial_t u_i + u_j\partial_j u_i - S(t)x_j\partial_j u_i - S(t)u_i - = -\partial_i\pi - \pi\partial_i\theta + ... \\ -\Pi^B(\mathbf{x},t)\partial_i\theta + \partial_j\left[\nu\left(\partial_j u_i + \partial_i u_j\right)\right] + \nu\left(\partial_j u_i + \partial_i u_j\right)\partial_j\theta \quad (2)$$

$$\partial_t\theta + \left(u_j - S(t)x_j\right)\partial_j\theta = \partial_j u_j \quad (3)$$

$$\partial_j u_j = -\partial_j\left(\mathscr{D}\partial_j\theta\right) \quad (4)$$

$$(5)$$

where u_i is the velocity perturbation, and where we introduce the new variables : $\theta = \log(\rho/\rho_{DT})$, the base reduced pressure Π^B and the reduced pressure perturbation π. The divergence of the velocity field is no longer zero as classically in variable density approximation (Sandoval (1995)). Equations 2 and 3 present inhomogenous and forcing terms, coming from the base velocity field. Nevertheless they can be eliminated using the rescaling of the space,time, velocity, pressure and θ as shown in Viciconte *et al.* (2018).

We solve these equations using a spectral collocation method Orszag & Patterson (1972). The simulation is advanced in time using a third order Runge-Kutta TVD Gottlieb *et al.* (2001). The effects of the plasma transport coefficients are taken into account using the particle-ion-in-jellium (PIJ) model, proposed by Arnault (2013), and further validated in Ticknor *et al.* (2016). The viscous contribution in the equation is taken into account implicitly, using the GMRES iterative method (Stoer & Bulirsch (2013)). In the following we use the overbar to indicate radial average defined as :

$$\overline{Q} = \int_0^{2\pi}\int_0^{\pi} Q(t,r,\phi,\psi)r^2 sin(\phi)d\psi d\phi$$

and the bracket to indicate volume average over the domain defined as :

$$\langle Q\rangle = \int Q(t,\mathbf{x})dV$$

Initial conditions

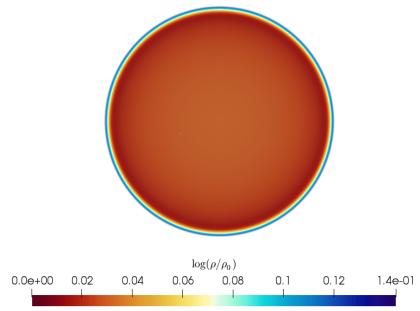

Figure 2: Initial contours of $\theta = \log(\rho/\rho_0)$.

In the configuration studied, the initial fuel/ablator interface radius is fixed at $300\mu m$. We specify a mean initial $\overline{\theta}$ radial profile by the Atwood number, $At = \frac{\rho_{CH}-\rho_{DT}}{\rho_{CH}+\rho_{DT}} = 0.08$ and an initial mixing layer width $5\mu m$.

Zero mean random perturbations of the velocity field are added around the interface. They are characterized by a typical length scale ℓ_0 and rms fluctuation u_0. Therefore, it is convenient to introduce the initial Reynolds number $\mathrm{Re}_0 = \frac{u_0\ell_0}{\nu}$ and an initial compression parameter $\mathrm{Cp}_0 = \frac{u_0}{\ell_0 S(0)}$.

TRANSPORT COEFFICIENTS EVOLUTION

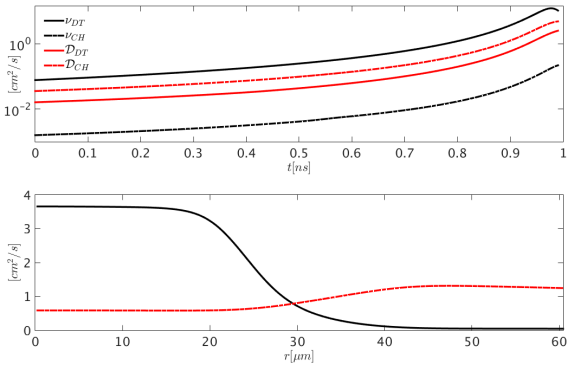

Figure 3: Evolution of the viscosity and diffusivity coefficients. Top: Evolution of ν and $\mathscr{D}$ outside the mixing layer during compression. DT and CH subscript indicates respectively values in the pure light and heavy materials. Bottom: Radial evolution of the averaged value of the transport coefficients at $R = 0.12$. Black: viscosity. Red: diffusivity.

During the compression, viscosity and diffusivity values vary due to the composition of the mixing layer, temperature and density. The transport coefficient temporal evolution is plotted at the top of figure 3. We observe that both viscosity and diffusivity values increase during the compression of almost three order of magnitude. Remark that due to heavier material mixing with pure fuel at the center of the capsule, ν_{DT} slightly decreases at the end of the simulation.

The radial profiles, at $R = 0.12$, are shown at the bottom of figure 3. The value of ν decreases of almost two orders of magnitude inside the mixing layer when it goes from light to heavy material. This difference grows during the compression, reaching almost three orders of magnitude. The evolution of $\mathscr{D}$ is the opposite. The diffusion decreases when passing from pure CH to pure DT, but its variation is not as important as for the viscosity.

RESULTS

First, we present the results from 512^3 grid points DNS with $\mathrm{Re}_0 = 240$ and $\mathrm{Cp}_0 = 0.006$, comparing simulations with plasma transport coefficients (PC) and constant (CC) ones. In the latter, we set ν and $\mathscr{D}$ to the $\nu_{CH}(t = 0)$, i.e. the value of the viscosity in the heavy material at the beginning of the simulation.
In figure 4, we present the comparison for θ contours, at different times. Beginning with the same initial condition in figure 2, we observe a striking difference between the two simulations. In fact, at time (I) the growth of transport coefficients already dissipates the small scales turbulent perturbations in the PC case, while they are still present in the CC simulation. This difference grows during the compression with the relaminarization of the layer in the PC computation that become more and more important. At time (III), no θ fluctuations are visible. In the case of CC simulation, turbulence is the main factor acting on θ, dominating the dynamics until reaching the minimum of the compression (corresponding to (III)).

One point statistics

The evolution of the total kinetic energy is plotted in figure 5 together with the variance of θ'. Here, $\theta' = \theta - \overline{\theta}$, that is, the fluctuations of the perturbation with respect of its mean radial value. At the beginning, in both simulations, the dynamics of the flow is determined by compression effects, leading to an increase of kinetic energy. This phase has been identified as a self similar regime in Viciconte *et al.* (2018) and called rapid compression regime. After this relatively short phase, CC and CP simulations start to differ. In the PC simulation, the kinetic energy $\mathscr{K}$ increases up to a point when the viscosity starts to affect the large scale of the flow triggering the sudden dissipation effect (see (Davidovits & Fisch, 2016)) after which, it enters a self similar viscous regime. In the CC simulation kinetic energy goes from the rapid compression regime to one where the nonlinear transfer are non negligible. This phase lasts until the end of the simulation when even with constant transport coefficients viscous effects become important.

We observe that the sudden dissipation effect acts as well on the scalar variance $\langle\theta'\theta'\rangle$. Dissipative phenomena act earlier on the scalar field compared to the velocity one, explaining the shift between the maximums. The smaller values of $\langle\theta'\theta'\rangle$ during the compression in PC simulations compared to CC ones suggest an enhanced mixing due to plasma transport coefficients.

Mixing layer width evolution

One central question in this work is the impact of plasma transport coefficients on the large scale behaviour of the mixing layer. In order to answer it, we need to quantify its growth. In this work we use the mixing layer width L, an integral quantity defined as function of the radial averaged mass fraction $\overline{Y}(r,t)$ (Andrews & Spalding (1990))

$$L(t) = 6\int \overline{Y}(t,r)(1-\overline{Y}(t,r))dr \tag{6}$$

In figure 6 we plot the evolution of L for CC and PC simulations, together with the PC reference case without turbulence *i.e* $Re_0 = 0$. Three phases can be identified in the mixing layer evolution for PC computation. At first turbulent diffusion dominates, and L grows similarly in PC and CC simulation, suggesting that transport coefficients have little effects. Later around $R = 0.5$, the two results start to differ. In this second phase the increase of viscosity and diffusivity increase the dissipation of turbulent fluctuations which entail the decrease of the turbulent diffusion, which at this point is still the dominant effect. This is the first effect of the transport coefficients on the mixing layer. In the third phase, around $L = 0.08$, the influence of the transport coefficients became dominant and they act at the mixing layer length scale. In fact this is the phase in which the results of the two simulations differ considerably.

Mixing quantification

In order to measure the mixing of heavy materials at the center of the capsule and identify how it is related to plasma transport coefficients, we introduce the following integral:

$$I_C(t) = \int_0^{R_c} Y_{CH}(\mathbf{x},t)dV \tag{7}$$

R_c is an arbitrary radius that we fix as the radius of the capsule. The results are plotted in figure 7. The trends of the mixing integrals follow that of the mixing zone width shown in figure 6. At the beginning the two results are on top of each other. Then after a second phase where the integral from CC simulation has a greater value than the one from PC data, there is a sudden diffusion phase where the mixing integral from PC simulation grows considerably, reaching almost twice the value of the result from the CC case .

Radial profile

In order to have more information on the spatial structure of the mixing layer, we look at the radial profiles of different quantities. In figure 8 we plot the heavy material mass fraction profile $\overline{Y}_{CH}$ at three different moment during compression. At the beginning, at $R = 0.12$ and at $R = 0.05$. From the same initial condition the two profiles evolve differently during the computations. In fact, we observe how in figure 8b the two profiles differ because the mixing layer in the constant coefficient simulation has been diffused more, thanks to the turbulence diffusion which is less intense in the PC simulation. Eventually at the end of the

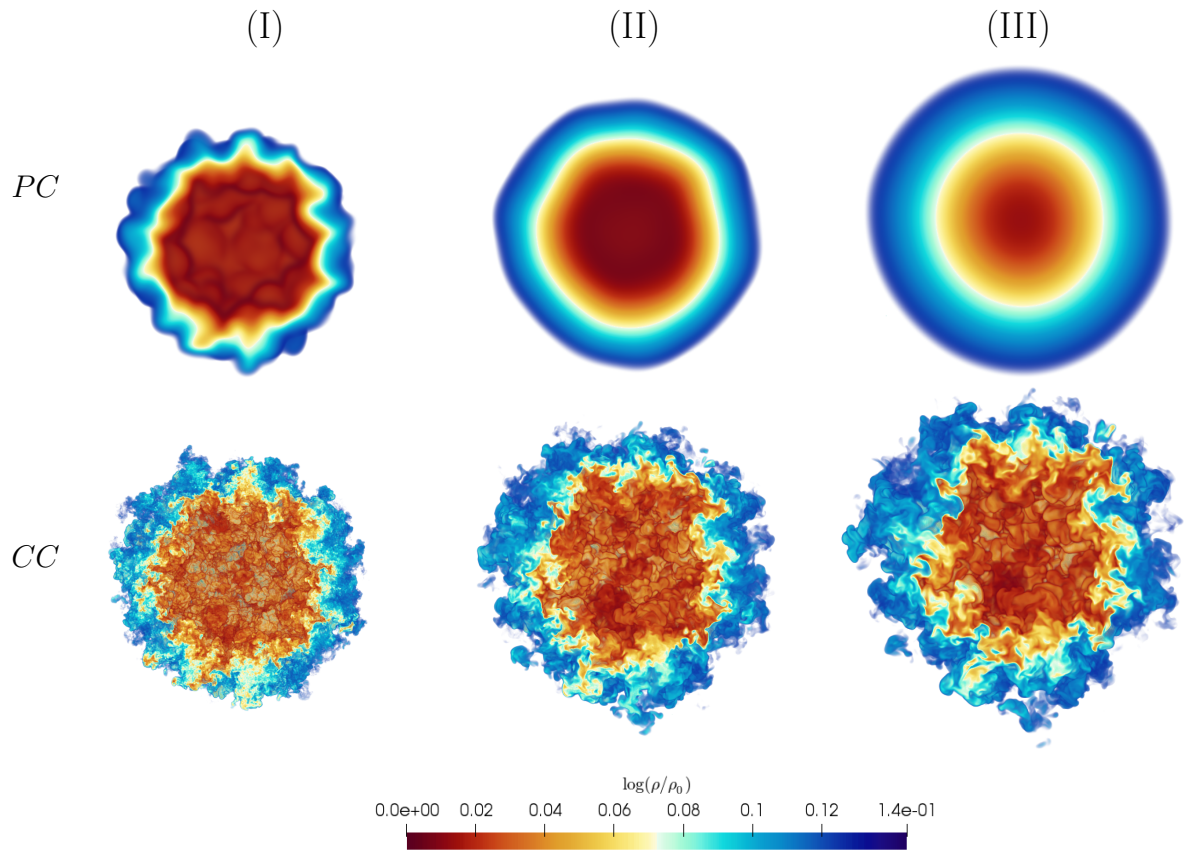

Figure 4: Comparison of contours of θ at three instants during compression. (I) at $R = 0.5$, (II) at $R = 0.08$, (III) at $R = 0.08$. Top evolution: with plasma transport coefficients (PC). Bottom evolution: with constant transport coefficients (CC).

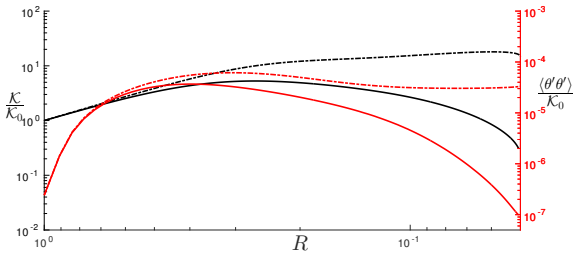

Figure 5: Evolution of the turbulent kinetic energy and $\langle\theta'\theta'\rangle$, normalized with the initial kinetic energy, as function of the compression parameter L. The continuous lines represent the case of plasma transport coefficients (PC). The dashed lines are for the constant case (CC).

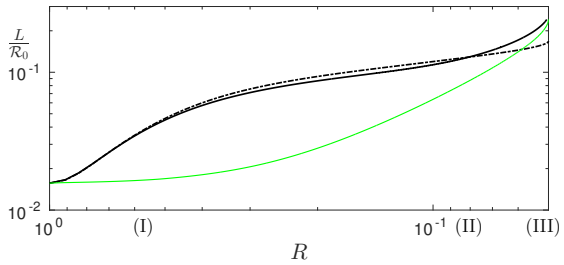

Figure 6: Evolution of the mixing layer width as function of the compression parameter R. Here L is normalized by the initial radius of the sphere. The continuous black line for the case of plasma transport coefficients (PC). The black dashed line is for the constant case (CC). The continuous green line is the reference case $\mathrm{Re} = 0$

compression, in figure 8c, we see that not only the mixing layer is wider for the *PC* simulation, but that the heavy material has moved toward the center of the domain. To confirm the difference in turbulent diffusion, we look a the profile of kinetic energy at the same instants as in 8, together with the radial variation of $\overline{\theta'\theta'}$. They are plotted in figure 9. The profile of $\mathscr{K}$ at $R = 0.12$ in figure 9b explain the difference that we see in 8b. In fact the values of kinetic energy for the CC simulation is greater than PC compression, implying a greater turbulent diffusion.

In figure 9c at the time of maximum compression, due to enhanced transport coefficients values, we observe that the fluctuations in the velocity as well as in θ fields have been dissipated. This is consistent with the data in figure 5 and the CC contour in 4.

In the simulation with plasma coefficients, we observe that the scalar variance peak move towards the center while the peak of kinetic energy moves towards the heavy material. This is due to the different behaviour of the transport coefficients in the mixing layer shown in figure 3.

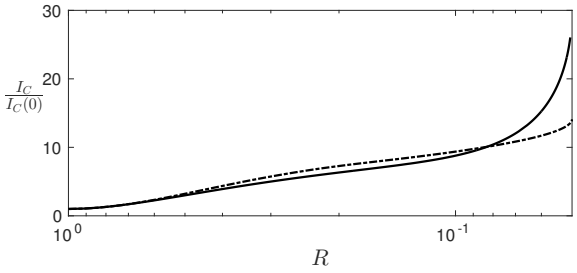

Figure 7: Evolution of the mixing integral value as function of the compression parameter R. Here I_C are normalized using their initial values. The continuous black line for the case of plasma transport coefficients (PC). The black dashed line is for the constant transport coefficients case (CC).

INITIAL CONDITION INFLUENCE

In this section, we wish to evaluate the effect of initial Reynolds number on the diffusion of the mixing layer. We perform a simulation at a lower initial Reynolds number $Re_0 = 60$. In the this case, the initial strong turbulent diffusion phase is absent, and the mixing layer growth is less intense than the previous computation. But in this case the sudden diffusion phase begin early . So that the difference between the mixing layer width in PC and CC simulations, in the final stage of the compression, is more important than in the previous cases. We remark the final size of the mixing layer in the case of the two PC simulations is the same and is consistent with the result at $Re = 0$.

CONCLUSIONS

In this work, we quantify mixing in imploding capsule relevant to idealized ICF configurations using direct numerical simulations accounting for plasma transport coefficients. Mixing zones originating from hydrodynamics instabilities at the fuel/ablator interfaces and transporting heavy materials toward the center evolve either by turbulent or physical diffusion. On the one hand, the tremendous viscosity growth during the compression decreases significantly turbulent diffusion. On the other hand, a sudden diffusion of the layer can be observed as the physical diffusivity overcome the turbulent one. Implementing transport coefficients in ICF simulation at low Reynolds number is therefore important to predict correctly the mixing.

REFERENCES

Andrews, M. J. & Spalding, D. B. 1990 A simple experiment to investigate twodimensional mixing by rayleigh-taylor instability. *Physics of Fluids A: Fluid Dynamics* **2** (6), 922–927.

Arnault, Philippe 2013 Modeling viscosity and diffusion of plasma for pure elements and multicomponent mixtures from weakly to strongly coupled regimes. *High Energy Density Physics* **9** (4), 711–721.

Betti, R & Hurricane, OA 2016 Inertial-confinement fusion with lasers. *Nature Physics* **12** (5), 435.

Braginskii, S. I. 1995 *Rev. Plasma Phys.* **1**, 205.

Cambon, C., Coleman, G. N. & Mansour, N. N. 1993 Rapid distortion analysis and direct simulation of compressible homogeneous turbulence at finite Mach number. *Journal of Fluid Mechanics* **257**, 641665.

Davidovits, Seth & Fisch, Nathaniel J. 2016 Sudden viscous dissipation of compressing turbulence. *Phys. Rev. Lett.* **116**, 105004.

Gottlieb, Sigal, Shu, Chi-Wang & Tadmor, Eitan 2001 Strong stability-preserving high-order time discretization methods. *SIAM review* **43** (1), 89–112.

Orszag, S. A. & Patterson, G. S. 1972 Numerical simulation of three-dimensional homogeneous isotropic turbulence. *Phys. Rev. Lett.* **28**, 76–79.

Remington, Bruce A, Park, Hye-Sook, Casey, Daniel T, Cavallo, Robert M, Clark, Daniel S, Huntington, Channing M, Kuranz, Carolyn C, Miles, Aaron R, Nagel, Sabrina R, Raman, Kumar S *et al.* 2018 Rayleigh–taylor instabilities in high-energy density settings on the national ignition facility. *Proceedings of the National Academy of Sciences* p. 201717236.

Rogallo, R. S. 1981 Numerical experiments in homogeneous turbulence. *Tech. Rep.* 81315. NASA, memo.

Sandoval, Donald Leon 1995 The dynamics of variable-density turbulence. PhD thesis, University of Washington.

Stoer, Josef & Bulirsch, Roland 2013 *Introduction to numerical analysis*, , vol. 12. Springer Science & Business Media.

Ticknor, Christopher, Kress, Joel D, Collins, Lee A, Clérouin, Jean, Arnault, Philippe & Decoster, Alain 2016 Transport properties of an asymmetric mixture in the dense plasma regime. *Physical Review E* **93** (6), 063208.

Viciconte, Giovanni, Gréa, Benoît-Joseph & Godeferd, Fabien S 2018 Self-similar regimes of turbulence in weakly coupled plasmas under compression. *Physical Review E* **97** (2), 023201.

Vold, E. L., Joglekar, A. S., Ortega, M. I., Moll, R., Fenn, D. & Molvig, K. 2015 Plasma viscosity with mass transport in spherical inertial confinement fusion implosion simulations. *Physics of Plasmas* **22** (11), 112708.

Weber, C. R., Clark, D. S., Cook, A. W., Busby, L. E. & Robey, H. F. 2014 Inhibition of turbulence in inertial-confinement-fusion hot spots by viscous dissipation. *Phys. Rev. E* **89**, 053106.

Zylstra, AB, Hoffman, NM, Herrmann, HW, Schmitt, MJ, Kim, YH, Meaney, K, Leatherland, A, Gales, S, Forrest, C, Glebov, V Yu *et al.* 2018 Diffusion-dominated mixing in moderate convergence implosions. *Physical Review E* **97** (6), 061201.

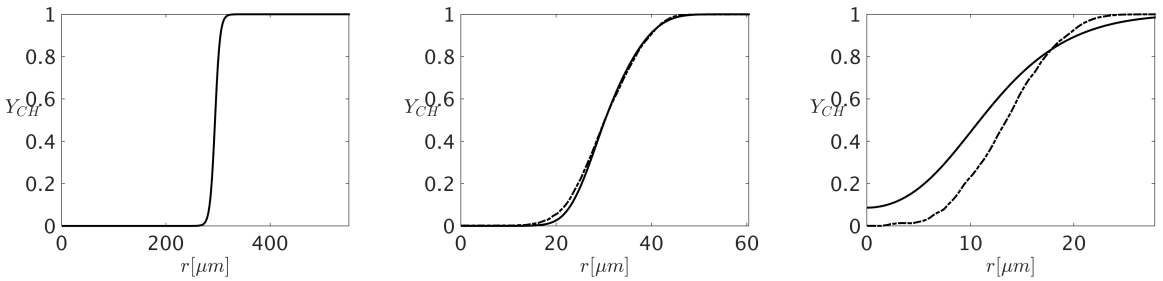

(a) $R = 1$ (b) $R = 0.12$ (c) $R = 0.05$

Figure 8: Heavy element (CH) radial averaged mass fraction Y_{CH} at three moments during compression. Continuous line for the *PC* simulation, dashed dotted line for the *CC* simulation.

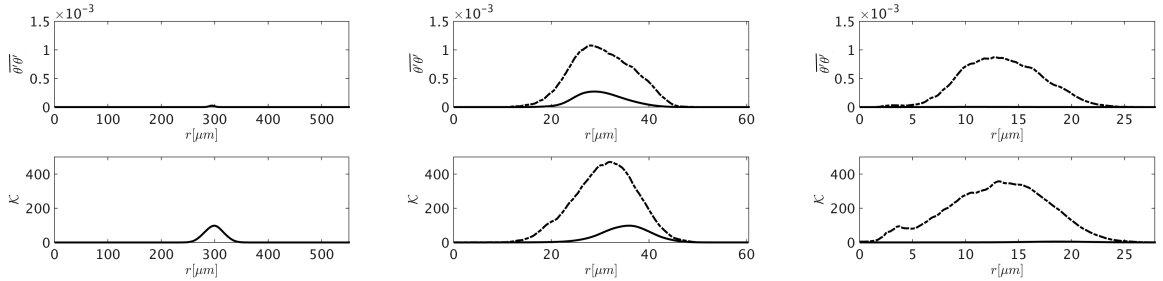

(a) $R = 1$ (b) $R = 0.12$ (c) $R = 0.05$

Figure 9: Radial profiles of the variance of θ (top) and kinetic energy (bottom), at three moments during compression. Continuous line for the *PC* simulation, dashed dotted line for the *CC* simulation.

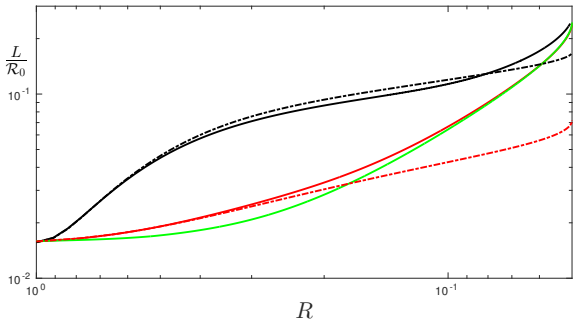

Figure 10: Evolution of the mixing layer width as function of the compression parameter R, for two different initial Re. Black lines : $Re = 260$ continuous line for the case of plasma transport coefficients (PC), dashed-dotted line is for the constant case (CC). Red lines : $Re = 60$ continuous line for the case of plasma transport coefficients (PC), dashed-dotted line is for the constant case (CC). The continuous green line is the reference case Re $= 0$